Applied Catalysis B: Environmental 224 (2018) 895–903

Contents lists available at ScienceDirect

Applied Catalysis B: Environmental

journal homepage: www.elsevier.com/locate/apcatb

Research paper

Structural and electronic properties of oxygen defective and Se-doped *p*-type $BiVO_4$(001) thin film for the applications of photocatalysis

Habib Ullah*, Asif A. Tahir*, Tapas K. Mallick

Environment and Sustainability Institute (ESI), University of Exeter, Penryn Campus, Penryn, Cornwall TR10 9FE, United Kingdom

ARTICLE INFO

Keywords:
Se-doped BiVO4
p-type semiconductor
Charge carriers
Water splitting

ABSTRACT

Monoclinic $BiVO_4$ is being used as a photocatalyst due to its stability, cost-effectiveness, ease of synthesis, and narrow band gap. Although, the valence band maximum, VBM (~ -6.80 eV vs vacuum) of $BiVO_4$ is well below the redox potential of water but having less positive conduction band minimum, CBM (-4.56 eV vs vacuum), responsible for its low efficiency. We have carried out a comprehensive periodic density functional theory (DFT) simulations for the pristine, Oxygen defective (O_v) and Se doped $BiVO_4$, to engineer not only its CB edge position but the overall photocatalytic and charge carrier properties. Our theoretical method has nicely reproduced the experimental data of pristine $BiVO_4$, which encouraged us to elaborate further its O_v and Se-doped characteristics. It is found that both the O_v (1% Oxygen vacancy) and Se-doped $BiVO_4$ (1–2% Se) have ideal band edges, band gaps, and small effective masses of electrons and holes, responsible for high photocatalytic activities. Moreover, Se-doped $BiVO_4$ behave as p-type semiconductor. Finally, the photocatalytic water-splitting behaviour of the selected surfaces were counterchecked with water interaction, where the strong water adsorption energy of about ~ -38 to -50 kcal/mol, confirms and predicts their higher efficiencies compared to that of parent $BiVO_4$.

1. Introduction

Solar energy harnessing via photoelectrochemical (PEC) water splitting, using transition metal oxides, is a direct chemical energy conversion and storage technique. Since the discovery of the first photocatalytic water splitting experiment, a range of transition metal oxides have been employed to produce solar fuel [1]. An ideal photocatalyst must have valance band (VB) and conduction band (CB), which straddle the redox potentials of photocatalytic reaction, and must have high stability, availability, and narrow band gap which can absorb efficiently the visible part of sun light [2,3].

$$O_2 + 4H^+ + 4e^- \rightleftharpoons 2H_2O \quad E_{anodic} = 1.23\ V\ (NHE)$$

$$4H^+ + 4e^- \rightleftharpoons 2H_2 \quad E_{cathodic} = 0\ V\ (NHE)$$

$$2H_2O \longrightarrow 2H_2 + O_2 \quad E_{rxn} = -1.23\ V$$

To date, the current focus semiconductors/photocatalysts are Fe_2O_3, $LaFeO_3$, TaON, $LaCrO_3$, $LaCoO_3$, TiO_2, $BiVO_4$, ZnS, ZnO_2, Bi_2WO_6, $SrTiO_3$, BiOX (Cl, Br, I), and etc. Some of these semiconductors have ideal band edges position but they are either unstable or having large band gaps, while some of them are narrow band gap but one of the band edges (either VB or CB) is situated at improper band edge energy (see Scheme S1) [4]. So, the redox reaction cannot be completed without the external bias potential (see reactions 1–3). Band structure engineering is one of the excellent strategies to tailor the band edges and band gaps of these semiconductors, through doping process [5–7].

Bismuth vanadate ($BiVO_4$) is a promising photocatalyst for solar energy conversion due to its nontoxic, low-cost, photostable, and eco-friendly nature. Generally, $BiVO_4$ has three different crystalline polymorphs: orthorhombic pucherite, tetragonal dreyerite, and monoclinic clinobisvanite [8]. These different polymorphs have different properties as the photocatalytic activity is strongly influenced by the crystal structure. For instance, the tetragonal $BiVO_4$ possesses a band gap of 2.9 eV and mainly absorbs UV region, while the monoclinic clinobisvanite (m-$BiVO_4$) exhibits a much higher photocatalytic activity due to its ideal band gap ($2.4-2.5$ eV) which absorb the UV and visible regions of the electromagnetic spectrum, having an ideal valence band edge position for driving water oxidation [9]. However, it has been recently reported that m-$BiVO_4$, an *n*-type semiconductor [10], exhibits poor photocatalytic property which is stem to low mobility of the photogenerated charge carriers (electron – hole pairs), positive potential of CB (vs NHE) and high charge recombination rates which

* Corresponding author.
E-mail addresses: hu203@exeter.ac.uk, habib_chemist@yahoo.com (H. Ullah), A.Tahir@exeter.ac.uk (A.A. Tahir).

https://doi.org/10.1016/j.apcatb.2017.11.034
Received 26 September 2017; Received in revised form 10 November 2017; Accepted 14 November 2017
Available online 16 November 2017

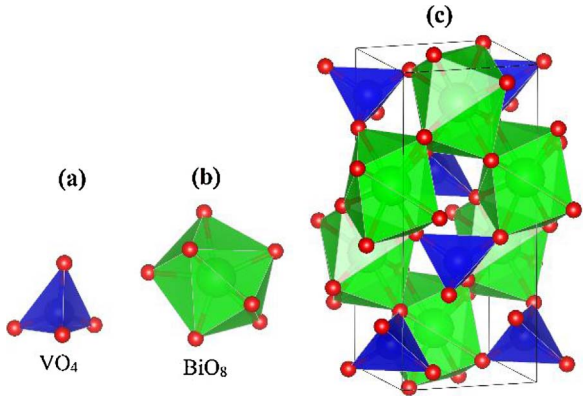

Fig. 1. Tetrahedral and dodecahedra geometries of VO_4 (a) and BiO_8 (b) in $BiVO_4$ (c).

significantly limit its practical applications. The photocatalytic activity of m-$BiVO_4$ can be tuned either with metal or non-metal doping, semiconductor recombination (heterojunction formation), depositing the co-catalysts, defect formation (oxygen vacancy creation), and crystal-facet control or morphological modification.

Moreover, it is important to investigate/design an efficient dopant for $BiVO_4$, which not only keeps its monoclinic crystal structure but to slow down the charge recombination rate and more negative CB (vs NHE) edge position. The monoclinic clinobisvanite structure of $BiVO_4$, consists of rows of isolated [VO_4] tetrahedra which are separated by the dodecahedral coordinated Bi atoms to form [BiO_8] with eight O atoms (Fig. 1).

In order to improve the overall photocatalytic activity of m-$BiVO_4$ (simply denoted as $BiVO_4$), different doping agents have been applied; these doping agents have either substituted the (I) V or (II) Bi atoms but no one has paid attention to substitute the (III) O site of $BiVO_4$. The previous literature of different doping agents [11–18], used for $BiVO_4$ can be summarized as!

(I). Doping of $BiVO_4$ at the V-sites is very common but due to different valence states of the dopant, a distortion in the [VO_4] tetrahedral chains cause phase transition from the parental monoclinic to tetragonal structure (Fig. 1). This distortion of [VO_4] tetrahedron chains in $BiVO_4$, plays a negative impact on the photocatalytic water-splitting, to generate H_2 gas. On the other hand, monoclinic $BiVO_4$ exhibits weak hole localization and is very helpful for water-splitting reaction. So, to keep the [VO_4] tetrahedral in the monoclinic structure of $BiVO_4$, Luo et al. have reported that ion doping with higher valence states such as Mo^{6+} and W^{6+}, to substitute V in $BiVO_4$, not only keep the parental geometry but also enhanced its photocatalytic activity [19].

(II). Another useful dopant agent which keeps the tetrahedral geometrical part of [VO_4] is Ce^{3+}, which substitutes the Bi^{3+} sites in $BiVO_4$. Ce^{3+} is a trivalent cation and has similar ionic radius to that of Bi^{3+}, substitutes the Bi-sites and not the V-sites (V^{5+}). Z. Jiang et al. have investigated that Ce^{3+} ions doped-$BiVO_4$ (Ce-$BiVO_4$) do not distort either the octahedral and dodecahedral geometries but act as trapping agent for the photogenerated holes which is responsible for the higher photocatalytic water oxidation activity compared to that of pristine one [20].

(III). No one has paid attention to substitute the O-sites in $BiVO_4$, and we believe that its substitution with di-anionic species such as selenium (Se^{2-}), with appropriate amount of doping ratio, will not disturb both the [VO_4] and [BiO_8] geometries. Furthermore, Se^{2-} would have dual attachment in the $BiVO_4$, coordinated with Bi on one hand and with V on the other side.

In this work, we investigated the effect of Oxygen vacancy and Se-dopant for the geometrical structure and corresponding photocatalytic activity of $BiVO_4$.

2. Computational methodology

First principle periodic boundary density functional theory (DFT) simulations are carried out, using Quantum ESPRESSO [21] and QuantumWise-ATK [22] while the results are visualized on VESTA [23] and vnl 2017.0 [24]. The experimentally observed crystallographic file of $BiVO_4$; clinobisvanite structure is used as such which has Hall symmetry space group of I2/b with lattice parameters of a = 5.147 Å, b = 5.147 Å, c = 11.7216 Å, and γ = 90° (See Fig. 1) [25]. Generalized gradient approximation (GGA) at Perdew-Burke-Ernzerhof (PBE) exchange-correlation functional is used for the structural and energy optimization [26]. As an input structure for the calculations; the 24 atoms primitive unit cell and its 2 × 2 × 2 supercell along with (001) direction with 10 Å vacuum, is considered as a model for the periodic boundary condition (PBC) DFT simulations. The local density approximation (LDA) method is found to be superior in reproducing the experimental data of $BiVO_4$, compared to pure GGA and meta GGA (MGGA). The detailed comparison of these methods is given in Supporting Information (Fig. S1 and S3). Generally, it is believed that clinobisvanite monoclinic $BiVO_4$ exists in (001) orientation so, that is why the (001) slab is opted for the theoretical simulations to represent its experimental thin film [27]. Moreover, the unreconstructed (001) termination possesses low surface energy and as a result represents the most probable surface termination [27]. Stability of these different slabs are confirmed from their positive formation energy and electrostatic potential; details of surface formation energy is give in Table S1 and Fig. S4-10 of the Supporting Information. A 5 × 5 × 1 Monkhorst-Pack k-grid and energy cutoff of 100 Ry is employed for the geometry relaxation and self-consistent (SCF) simulations of $BiVO_4$; consisting of 96 atoms. The Broyden-Fletcher-Goldfarb-Shanno algorithm (BFGS) is used for the structural relaxation [28]. A 5 × 5 × 5 Monkhorst-Pack k-grid with the same energy cutoff is used for the non-SCF part to get the density of states (DOS) and partial DOS (PDOS). The band structure simulations were performed along the direction of Γ, Z, R, X, and M of the Brillouin zone. The valence electron configurations considered are: $5d^{10}$ $6s^2$ $6p^3$ for Bi; $3p^6$ $3d^3$ $4s^2$ for V; $2s^2$ $2p^4$ for O, $1s^2$ for H, and $4s^2$ $4p^4$ $3d^{10}$ for Se atom.

3. Results and discussion

3.1. Optimized structures of pristine, oxygen defective, and Se-Doped $BiVO_4$(001)

The removal of an oxygen atom, and Se dopant on the tetrahedral or dodecahedra geometries of monoclinic clinobisvanite is investigated from the resulting relaxed geometries. Optimized structures of these different species of $BiVO_4$ are given in Fig. 2, where the bond distances between V—O and Bi—O decrease; considering the case of O_v and Se-doped $BiVO_4$(001). When the Se dopant ratio is increased from 2 to 3 or 4, it distorted the geometries of parent $BiVO_4$(001) as can be seen from Fig. 2. However, in case of 1–2% doping ratios, the resulted geometries were quite compact and similar to parent $BiVO_4$(001).

3.2. Electronic properties

3.2.1. Electronic properties of BiVO4(001) surface

As discussed in our previous report [29], that the monoclinic clinobisvanite phase exhibits a much higher photocatalytic activity compared to its other polymorphs due to its favourable band gap (2.4 − 2.5 eV) in the visible region of electromagnetic spectrum and a valence band position suitable for driving water oxidation [9].

The electronic properties such as DOS/PDOS and band structure of $BiVO_4$(001) are given in Fig. 3, where its band gap is 2.24 eV. This band gap is about 0.16 eV smaller than that of experimental but it is expected from LDA [30], which underestimate the band gap. However, it has nicely reproduced both the VB and CB edge positons of pristine

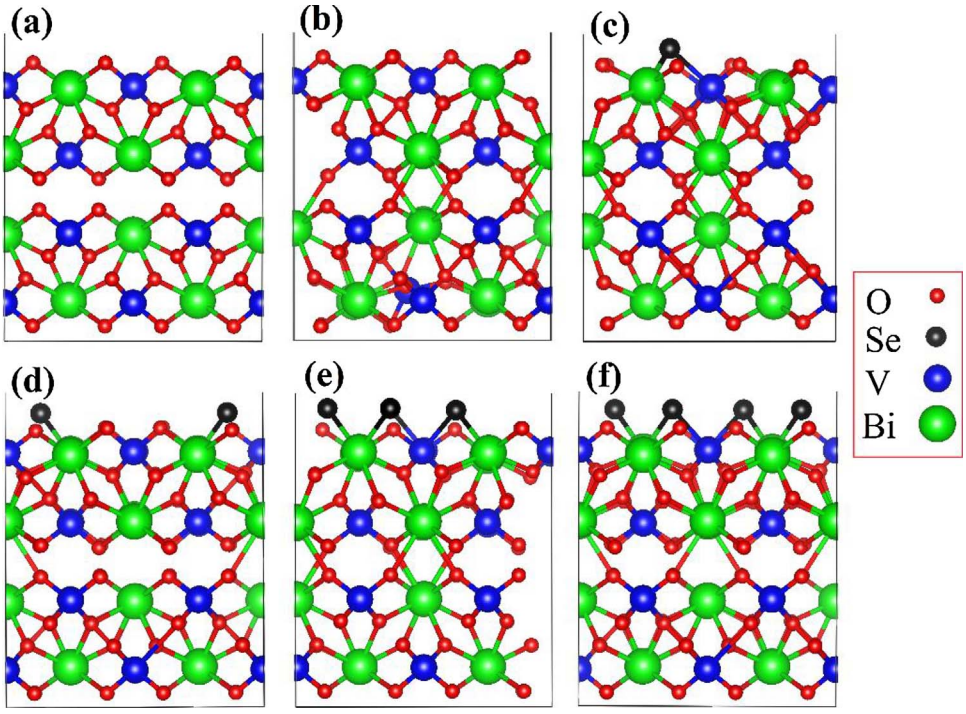

Fig. 2. Relaxed structures of (a) $BiVO_4$(001), (b) Ov, (c) 1%, (d) 2%, (e) 3%, and (d) 4% Se doped $BiVO_4$(001).

$BiVO_4$(001); ca. at −6.80 eV and −4.56 eV (vs vacuum), respectively. Analysis of the PDOS led us to conclude that orbitals of O atoms are responsible for developing valence band edge, however, the conduction band edge is that of V atoms. Contribution of the s, p, and d orbitals of Bi, V, and O, in making the band gap and edge positions are given in Fig. S11 of the Supporting Information. The s and p orbitals of Bi atoms consititute VB and CB edge of Bi, 3d orbitals of V are responsible for its VB and CB while in case of O, 2p orbitals have a major role in developing their band edge positions. Band structure of the $BiVO_4$(001) along the k-points direction of Γ, Z, R, X, and M is given in Fig. 3, where an indirect band gap of 2.24 eV has good agreement with the experimental and recently theoretical reported data [9]. Fruthermore, the simulated band edge energies (VBM ~ −6.80 and CBM ~ −4.56 eV at vacuum level) of $BiVO_4$ indicate that its CBM need to be engineered for high PEC performance. The effective masses of the photogenerated electrons (m_e^*) and holes (m_h^*) along the X → Γ directions of k-points are calculated by fitting parabolic approximation around the bottom of the CBM or the top of the VBM, respectively; using Eq. (1) (Table 1):

$$m^* = \hbar^2 \left(d^2 E/dk^2\right)^{-1} \quad (1)$$

where $\hbar$ is the reduced Planck constant, E is the energy of an electron at wave vector k in the same band (VBM or CBM). The simulated values of the effective masses of photogenerated electrons and holes of the $BiVO_4$(001) are 0.09 and 0.28 m_e, respectively.

The integrated local DOS (ILDOS) of $BiVO_4$(001) within various energetic windows of the VBM, CBM, band gap, and electrostatic potential (ESP) are presented in Fig. 4. The ILDOS at the CBM (0 − 1.6 eV), as well as a cross section of the ILDOS through the (001) plane highlights the primary contribution from V orbitals which can be found from Fig. 3 and Fig. S11. Localization of CBM electrons is because of the poor hybridization of V neighbouring orbitals as can be seen from Figs. 3, 4 and S11. The poor photoelectrochemical performance $BiVO_4$ thin film can be correlated with poor hole mobility (effective mass of hole ~0.28 m_e) rather than electron, which limits photocarrier transport and charge extraction. The self-trapping and small electron polaron formation in this material is due to the localization of photogenerated hole. Pristine $BiVO_4$(001) is an *n*-type semiconductor where the electrons play an important role in the photocatalytic reaction. This statement also corroborate the already reported work of A. Rettie et al. [31] So, the relative delocalized orbitals at CBM compared to VBM (Fig. 3) confirmed that majority of hole, limit the charge transport in

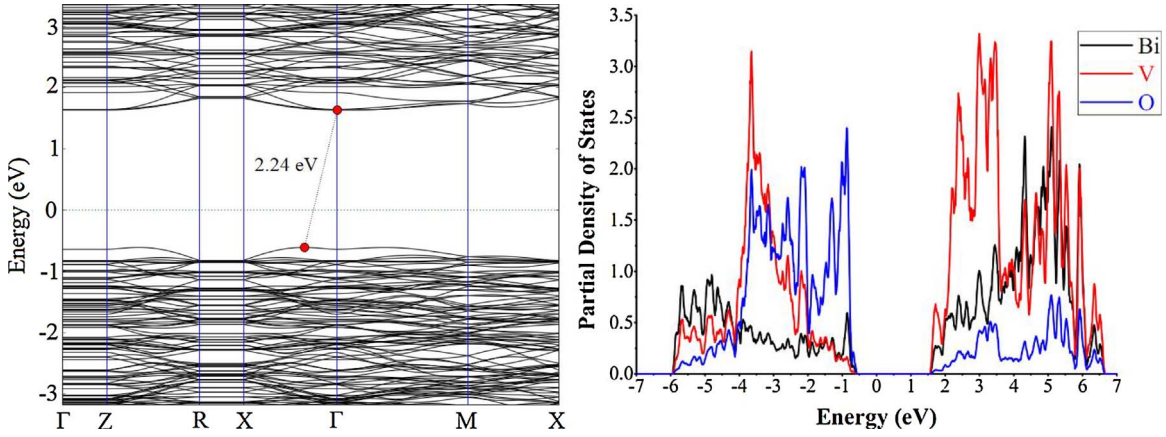

Fig. 3. Band Structure and PDOS plot of $BiVO_4$(001); the Fermi energy is set to zero.

Table 1
Fermi energy, % doping, VBM, CBM, Band Gap, and Effective Masses of Photogenerated Electrons and Holes, Estimated from the calculated Band Structure along the suitable direction.

Species	*Fermi Energy*	*% Doping*	m_e^*/m_o	m_h^*/m_o	*VBM*	*CBM*	*Band gap*
$BiVO_4$(001)	−6.18	Pure	0.09	0.28	−6.80	−4.56	2.24
O_v_$BiVO_4$	−4.28	1.0	0.19	0.18	−6.29	−4.33	1.96
1Se_$BiVO_4$(001)	−5.17	1.04	0.09	0.02	−5.80	−4.41	1.39
2Se_$BiVO_4$(001)	−5.19	2.08	0.04	0.31	−5.81	−4.08	1.73
3Se_$BiVO_4$(001)	−4.93	3.0	0.65	2.02	−5.47	−4.39	1.08
4Se_$BiVO_4$(001)	−4.73	4.16	0.01	0.24	−5.38	−4.14	1.24

this material.

3.3. Electronic properties of oxygen vacancy $BiVO_4$(001) surface

In order to understand the effect of oxygen vacancy (O_v) on the photoelectrochemical performance of $BiVO_4$, 1% O_v_$BiVO_4$(001) is employed for DFT simulations. The VB and CB orbitals distributions are almost similar to that of parent slab, however, the Fermi energy merge in the CB which is due to the extra electron(s) of the O_v, as can be seen from Fig. 5. It is also reported that monoclinic $BiVO_4$ is normally an intrinsic *n*-type semiconductor [32]. The contribution of V, Bi, and O orbitals are comparatively given in Fig. S12 of the Supporting Information. In this case, the electrons (0.19 m_e) are said to be the "majority carriers" for current flow (behave as an *n*-type semiconductor) while the effective mass of holes is 0.18 m_e. Overall, small effective masses of electrons and holes are estimated from the CBM and VBM of O_v_$BiVO_4$(001) compared to that of parent slab. At vacuum level, the CBM and VBM are −6.29 and −4.33 eV, which are well above and below the redox potential of water, respectively (Table 1). Moreover, electron doping (Oxygen vacancy creation) of $BiVO_4$ has not only reduced its band gap, but shift the CB to more positive potential (vs vacuum) as can be seen from Table 1.

3.4. Electronic properties of Se-Doped $BiVO_4$(001) surfaces

In order to improve the photocatalytic performance of $BiVO_4$, Se is incorporated in the form of different dopant concentrations. Oxygen atom(s) is substituted with Se in $BiVO_4$(001), from 1 to 4% dopant ratios, denoted as 1Se, 2Se, 3Se and 4Se_$BiVO_4$(001). 1% Se-doped has excellently improved the visible light absorption of $BiVO_4$(001) as can be seen from its band gap reduction, from 2.24 to 1.39 eV (Fig. 6 and Table 1). Moreover, p orbitals of Se constitute the VB of 1Se_-$BiVO_4$(001), as can be seen from its PDOS plot (Fig. 6). The individual PDOS plots of Bi, V, O, and Se are shown in Fig. S13 of the Supporting Information. Se has not only reduced the band gap of parent $BiVO_4$, but changed both the VB and CB, to −5.80 eV and −4.41 eV (vs vacuum), respectively. Compared to parent $BiVO_4$(001), 1Se_$BiVO_4$(001) has an ideal CBM position which is well above the redox potential of water, responsible for water reduction. Se is a *p*-type dopant, which has produced some flat bands in the VB of parent $BiVO_4$(001), however, it has

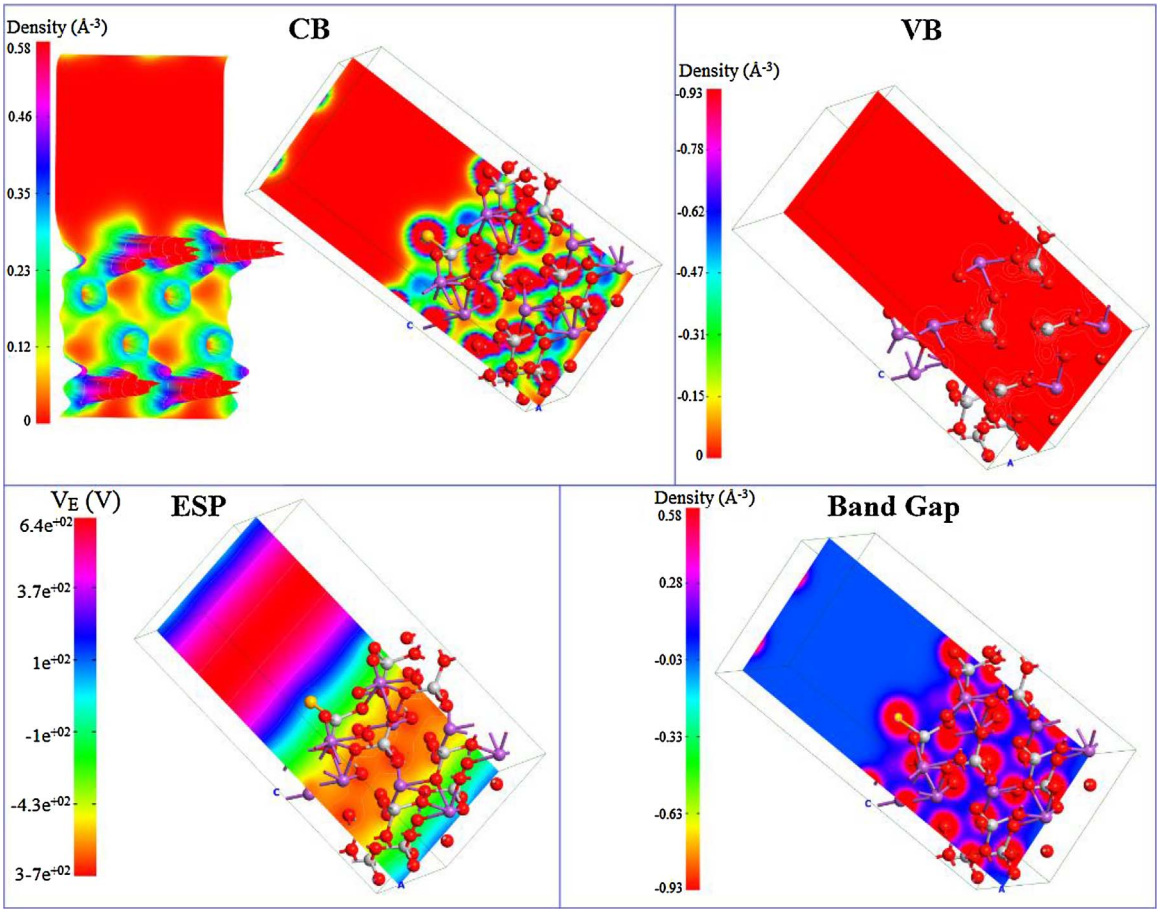

Fig. 4. Integrated local density of states of CBM, VBM, Band gap and ESP of $BiVO_4$(001).

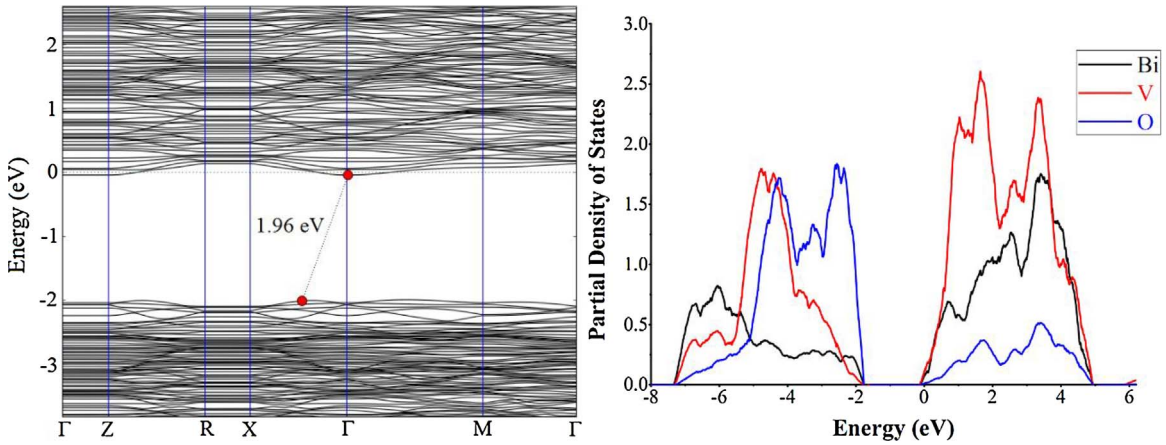

Fig. 5. Band Structure and PDOS plot of O_v_$BiVO_4$(001); the Fermi energy is set to zero.

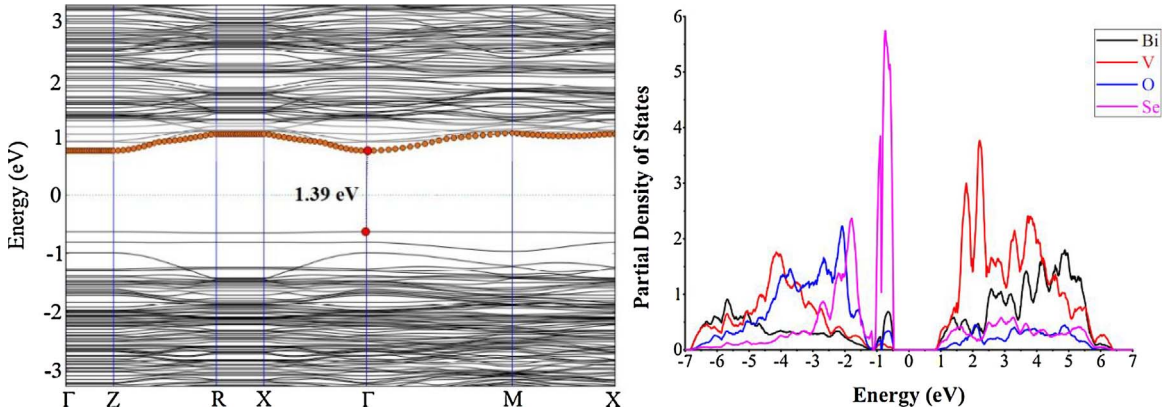

Fig. 6. Band structure and PDOS of 1% Se_$BiVO_4$(001); the Fermi energy is set to zero.

significantly reduced the effective masses of electrons and holes (Table 1). The effective masses of these photocarriers are 0.09 m_e for electron and 0.02 m_e of hole (Note: for the effective masses of hole, we considered the third band, below the VBM). On the other hand, flat band of VB produces an effective mass of holes of about 7.12 m_e, which are responsible for stationary holes. In summary, the high DOS in the VB Fermi level shift towords CB is clear evidence of the *p*-type nature of 1Se_$BiVO_4$(001). Moreover, 1Se_$BiVO_4$(001) can be used as a best photocatalyst for solar water splitting due to its ideal band edges positions, narrow band gap, and small effective masses of charge carriers (*vide infra*).

In the searching of an optimum dopant ratio of Se, to design an efficient photocatalyst, we also considered the 2Se_$BiVO_4$(001) system. The simulated band structure and PDOS of 2Se_$BiVO_4$(001) are given in Fig. 7, while its comparative PDOS plot for Bi, V, O, and Se atoms are given in Fig. S14 of the Supporting Information. Again, the VB and CB are made of Se and V atoms, respectively. The VB and CB of 2Se_$BiVO_4$(001) are situated at −5.81 and −4.08 eV (at vacuum), respectively which result band gap of 1.73 eV. Moreover, the simulated effective masses of electrons and holes are 0.04 m_e and 0.31 m_e, respectively, which predict high carrier mobility and charge separation rate. Very similar to 1Se_$BiVO_4$(001), 2Se_$BiVO_4$(001) also behave as a *p*-type semiconductor as can be seen from its band structure and PDOS plot. So, both the 1 and 2% Se doped $BiVO_4$(001) have almost similar photocatalytic characteristics and can be used for efficient water splitting, especially for water reduction.

The effect of 3 and 4% Se on $BiVO_4$(001) and their band gap and effective masses of charge carriers are contrast to that of 1 and 2%, as can be seen from Table 1 and Fig. 8. For simplicity reason, the band gap and orbitals contribution of Bi, V, O, and Se of 3 and 4% Se-doped $BiVO_4$(001) are given in Fig. S15-S18 of the Supporting Information. Although, this higher doping concentration has well reduced the bandgap of parent $BiVO_4$(001), 1.08 eV for 3 and 1.24 eV for 4% Se, but on the other hand it has sufficiently increased the VB and CB values (vs vacuum). The CBM positions of both these systems is well above the redox potential of water (vs vacuum) but the VBM is not able to perform the oxidation of water, to complete the overall water splitting reaction. The VBM and CBM of 3Se_$BiVO_4$(001) are −5.47 and −4.39 eV while that of 4Se_$BiVO_4$(001) are −5.38 and −4.14 eV, respectively. For the effective masses of charge carriers of these two systems, see Table 1.

Comparative analysis of the Oxygen defective and Se doped (1–4%) $BiVO_4$(001), led us to conclude that both the defective and mild (1 and 2%) Se-Doped $BiVO_4$(001) are best candidates for photocatalytic water splitting, based on their simulated VB, CB, Bandgap and effective masses of charge carriers.

3.5. Adsorption of water on pristine, oxygen defective, and 1% Se doped $BiVO_4$(001)

In order to elaborate the photocatalytic performance of the titled species, we adsorb water molecules on the surface of pristine, O_v_ and 1Se_$BiVO_4$(001), see Fig. 9 for their relaxed structures. Two molecules of water are adsorbed on each of these surfaces, optimized and followed by electronic properties simulations such as bandgap, band edge and effective masses of charge carriers. The adsorption energy of water molecules is simulated with the help of Eq. (1), by subtracting the energies of the optimized water molecule and adsorbent bare slab (E_{slab}) from the optimized water-slab complex (slab@water), using Eq. (1).

$$\Delta E_{ad} = E_{slab@water} - (E_{water} + E_{slab}) \quad (1)$$

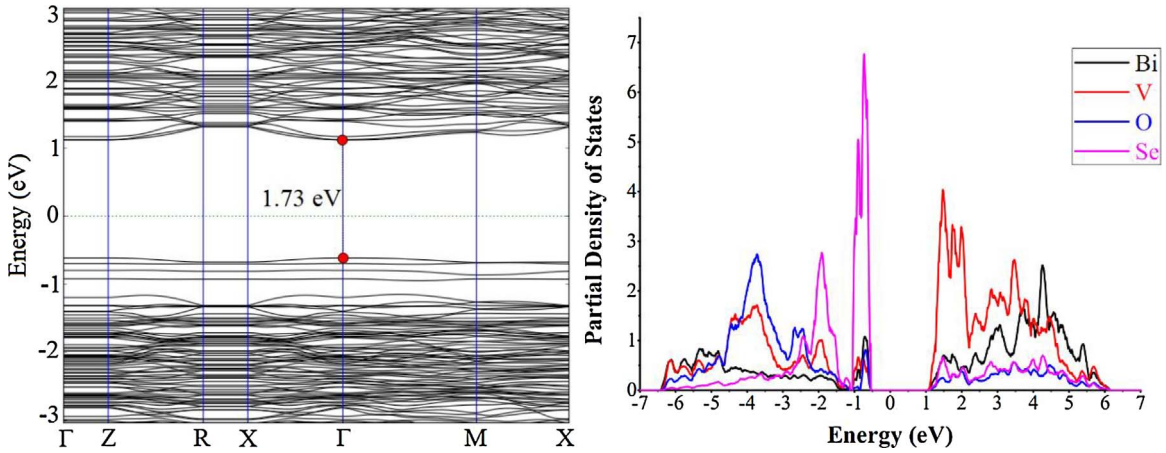

Fig. 7. Band Structure and PDOS plot of 2% Se_$BiVO_4$-001; the Fermi energy is set to zero.

3.6. Pristine BiVO4(001)@H2O

In case of $BiVO_4$(001)@H_2O, one of the water molecules is more attracted towards the surface via O—Bi and two H—O bondings, having distances of 2.45 and 1.62 Å, respectively (Table 2).

Hydrogen atoms of water molecules make a strong hydrogen bonding with the surface O atoms of $BiVO_4$(001), consequences the water splitting ability of pristine $BiVO_4$. The parent H—O bond distances (0.97 Å) and H—O—H angle (102°) of water molecule enlarged to 1 Å and 110.41°, respectively when H_2O is adsorbed on the (001) surface of $BiVO_4$. The per-water molecular adsorption energy is −38.28 kcal/mol, responsible for H_2O splitting over (001) surface of $BiVO_4$. Moreover, the negative ΔE_{ad} value indicates an exothermic adsorption process.

The electronic band structure and PDOS plot of $BiVO_4$(001)@H_2O are given in Fig. 10, where the band gap of parent BiVO4(001) is reduced to 1.74 eV upon adsorption of water molecules. So, the bandgap reduction of 0.48 eV confirm the water affinity of $BiVO_4$ towards its (001) surface. From the band structure and PDOS (Fig. 10) of $BiVO_4$(001)@H_2O system, it can be concluded that the VB orbital of water molecules has strong hybridization with the VB of $BiVO_4$(001). Comparative analysis of the data of Table 1 and Fig. 10, led us to conclude that the water has moved the VB of pristine $BiVO_4$(001) from −6.80 to −5.96 eV and CB from −4.56 to −4.22 eV, at vacuum level. The individual PDOS plots of Bi, V, O, and H_2O is given in Fig. S19 of the Supporting Information. In summary, the strong adsorption energy, perturbation in both inter, and intra-bond distances of water and $BiVO_4$(001), confirmed and validate the already experimental photocatalytic ability of $BiVO_4$ [33,34].

3.7. Oxygen defective BiVO4(001)@H2O

As discussed earlier, the Oxygen defective $BiVO_4$(001) has ideal band edge positions (well above and below the redox potential of water) and narrow band gap to be used as photocatalyst for water splitting. This defective surface has strong attraction for water molecules as can be observed from its adsorption energy (−50.85 kcal/mol). However, the inter-bond distances of H—O and Bi—O are longer compared to that of pristine@H_2O system. The reason behind this is, the more electropositive nature of O_v_BiVO4(001) surface (especially O and Bi atoms), results weak hydrogen and electrostatic type of bondings (Table 2). In O_v_BiVO4(001), the H—O bond distances of water molecules elongate to 0.99 Å, which result its further dissociation, as can be seen from Fig. 9b. The inter-bond distances such as the H—O (H of water and O of surface) are became enlarged which can be regarded to the cationic nature of O defective surface of $BiVO_4$(001).

Upon adsorption of water molecules on the Oxygen defective surface, the band gap of the resulted specie increases from 1.96 to 2.28 eV, as can be seen from Fig. 11 and Table 1 and 2. This 0.32 eV bandgap enlargement is due to the shifting of CB, which is about 0.38 eV compared to parent slab as can be seen from the PDOS of O_v_$BiVO_4$(001). Contrast to $BiVO_4$(001)@H_2O system, here water molecules has sufficiently changed the energy of CB of O_v_$BiVO_4$(001). The strong interaction of water with the O defective surface can be analysed from its

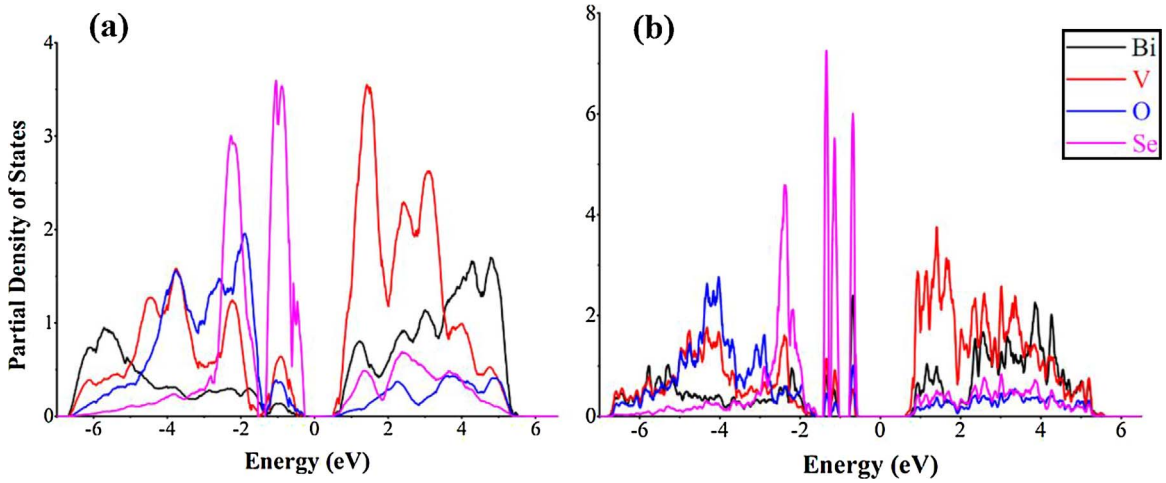

Fig. 8. PDOS plot of (a) 3Se and (b) 4Se_$BiVO_4$(001); the Fermi energy is set to zero.

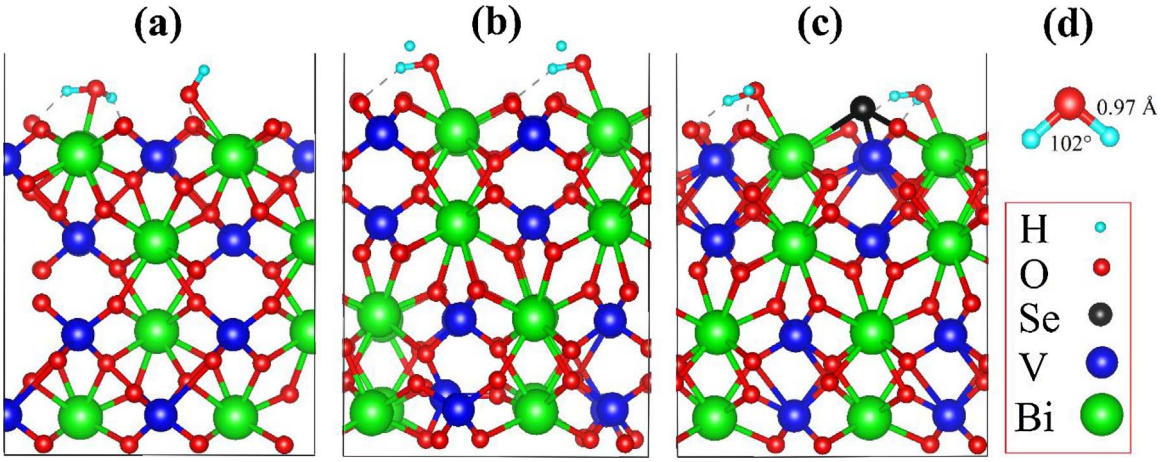

Fig. 9. Relaxed structure of (a) $BiVO_4(001)@H_2O$, (b) O_v_$BiVO_4(001)@H_2O$, (c) 1Se_$BiVO_4(001)@H_2O$, and (d) water.

Table 2
Inter-bond distance, Water Adsorption Energy (E_{ad}), and Bandgaps of Water Adsorbed-$BiVO_4(001)$, Ov, and 1Se_$BiVO_4(001)$ Systems.

Species	$H_{(water)}$—$O_{(surface)}$ (Å)	$Bi_{(surface)}$—$O_{(water)}$ (Å)	E_{ad} (kcal/mol)	*Band gap*
$BiVO_4(001)@H_2O$	1.62	2.45	−38.28	1.74
O_v_$BiVO_4@H_2O$	1.75	2.51	−50.85	2.28
1Se_$BiVO_4@H_2O$	1.59	2.45	−40.24	1.35

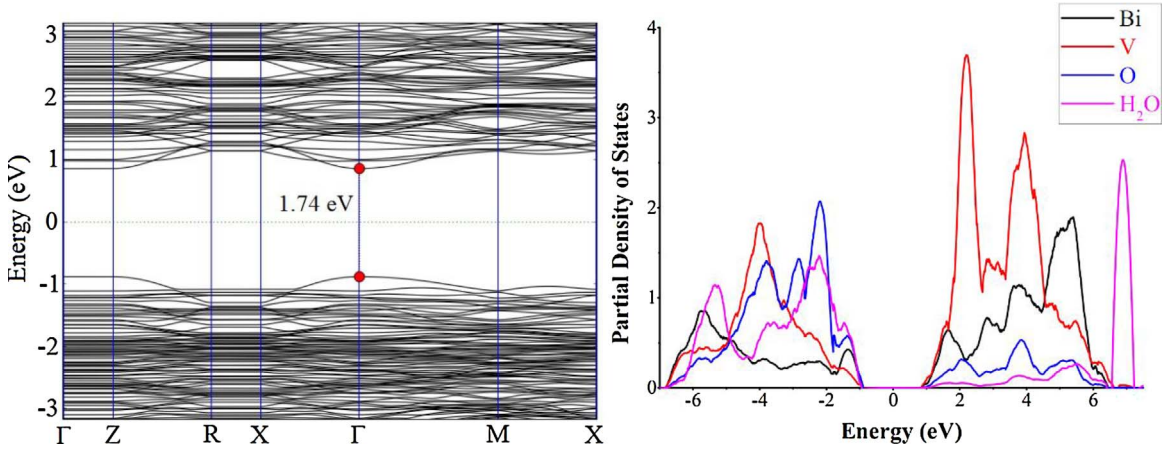

Fig. 10. Band Structure and PDOS plot of $BiVO_4$-001@H_2O; the Fermi energy is set to zero.

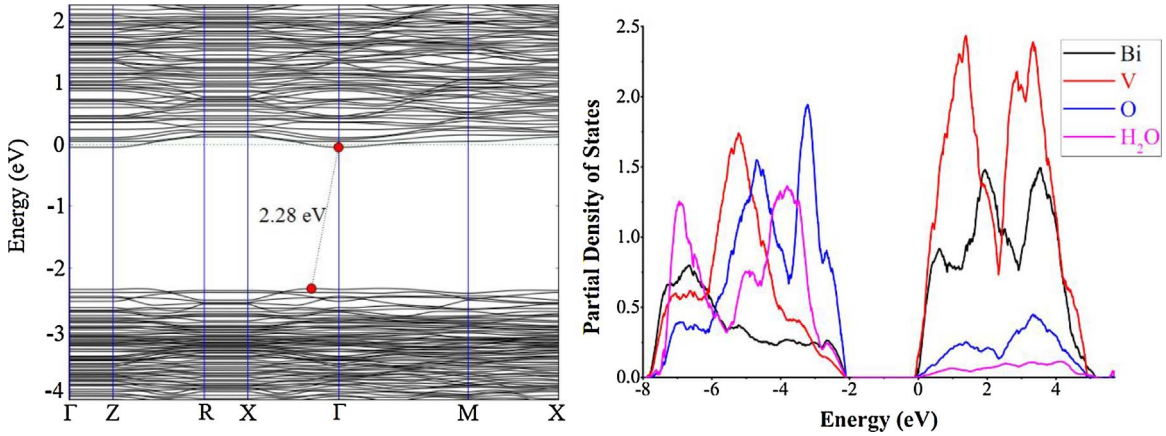

Fig. 11. Band structure and PDOS of O_{vac}_$BiVO_4(001)@H_2O$; the Fermi energy is set to zero.

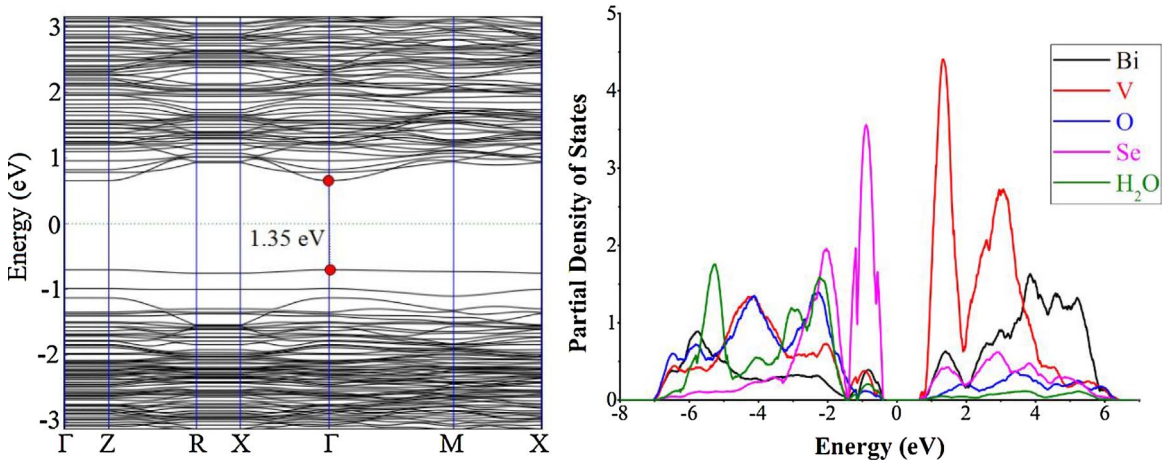

Fig. 12. Band structure and PDOS of 1Se_$BiVO_4$(001)@H_2O; the Fermi energy is set to zero.

highest adsorption energy (−50.85 kcal/mol) and orbital overlapping, especially in the VB of O_v_$BiVO_4$(001)@H_2O system (Fig. 11). The individual PDOS plots of Bi, V, O, and H_2O are given in Fig. S20 of the Supporting Information.

3.8. 1% Se-Doped-BiVO4(001)@H2O

Finally, the water adsorption on the 1Se_$BiVO_4$(001) surface is investigated, where its optimized parameters are given in Table 2 and electronic properties in Fig. 12 and S21. The simulated water adsorption energy (−40.24 kcal/mol) led us to conclude that 1% Se doped $BiVO_4$(001) can be easily used an efficient photocatalytic material. Furthermore, the inter-Hydrogen bonding and electrostatic bond distances are 1.59 and 2.45 Å, respectively, which confirm the enhanced catalytic ability of Se doped $BiVO_4$. Besides these geometric parameters, electronic properties of the resulting system are also effected, upon adsorption of water molecules. Both the VB and CB are slightly moved from its parental position, which has decreased the overall band gap, from 1.39 to 1.35 eV as can be seen from Fig. 12 and Table 2.

In summary, although pristine $BiVO_4$ is a good photocatalyst for water splitting, having narrow bandgap and VB edge position, but inappropriate CB potential, reduces its hydrogen evaluation efficiency. This comprehensive theoretical simulation predicts that both the Oxygen defective and mild doped (1 or 2% Se) $BiVO_4$ have not only changed the band edges positions (well above and below the redox potential of water) but reduced the bandgap as well, results a champion photocatalyst for water splitting.

4. Conclusion

We have carried out a comprehensive periodic density functional theory (DFT) simulations for the pristine, oxygen defective (O_v) and Se-doped $BiVO_4$(001), to improve its photocatalytic performance. $BiVO_4$ is a stable, cheap, easily synthesizable, having appropriate band gap and valance band (VB) edge position but less positive conduction band (CB) edge position (vs vacuum). Our theoretical simulations of $BiVO_4$(001) surface has nicely reproduced the experimental data which has validated and confirm the method used. Furthermore, it is found that O_v (1%), and Se-doped (1–2%) $BiVO_4$(001) have narrowed band gaps, small effective masses of electrons and holes, and well above and below CBM and VBM, respectively (in line with the redox potential of water). Moreover, Se-doped $BiVO_4$(001) behave as a *p*-type semiconductor, capable of H_2 production from water reduction. Finally, the selected surfaces were interacted with water molecules, to check their water absorption energy. The water adsorption energies vary as O_v_$BiVO_4$(001)@H_2O > 1Se_$BiVO_4$(001)@H_2O > $BiVO_4$(001)@H_2O. Although, Oxygen defective (1% O vacancy) $BiVO_4$(001) has narrow band gap (1.96 eV), suitable redox potentials (VB −6.29 eV, CB −4.33 eV at vacuum level), and high-water adsorption energy but thermodynamically less stable compared to Se-doped $BiVO_4$(001). So, we conclude and predict that mild doped Se_$BiVO_4$(001) is not only stable but can efficiently absorb the visible part of sun light and split water into O_2 and H_2 without any external biased.

Acknowledgment

The financial support was provided by Engineering and Physical Science Research Council, UK (EPSRC) under the research grant No EP/P510956/1. We also acknowledge Dr Andrew Cowley (Computing Development Officer) for the assistance of supercomputing facilities of ESI Beowulf Cluster.

Appendix A. Supplementary data

Supplementary data associated with this article can be found, in the online version, at http://dx.doi.org/10.1016/j.apcatb.2017.11.034.

References

[1] A. Fujishima, Electrochemical photolysis of water at a semiconductor electrode, Nature 238 (1972) 37–38.
[2] M.G. Walter, E.L. Warren, J.R. McKone, S.W. Boettcher, Q. Mi, E.A. Santori, N.S. Lewis, Solar water splitting cells, Chem. Rev. 110 (2010) 6446–6473.
[3] T. Hisatomi, J. Kubota, K. Domen, Recent advances in semiconductors for photocatalytic and photoelectrochemical water splitting, Chem. Soc. Rev. 43 (2014) 7520–7535.
[4] J. Li, N. Wu, Semiconductor-based photocatalysts and photoelectrochemical cells for solar fuel generation: a review, Catal. Sci. Technol. 5 (2015) 1360–1384.
[5] H. Ullah, Inter-molecular interaction in Polypyrrole/TiO_2: a DFT study J, Alloys Compd. 692 (2017) 140–148.
[6] H. Ullah, A.A. Tahir, T.K. Mallick, Polypyrrole/TiO_2 composites for the application of photocatalysis, Sens. Actuators B 241 (2017) 1161–1169.
[7] X. Jia, J. Cao, H. Lin, M. Zhang, X. Guo, S. Chen, Transforming type-I to type-II heterostructure photocatalyst via energy band engineering: a case study of I-BiOCl/I-BiOBr, Appl. Catal. B: Environ. 204 (2017) 505–514.
[8] M.D. Rossell, P. Agrawal, A. Borgschulte, C. c. Hébert, D. Passerone, R. Erni, Direct evidence of surface reduction in monoclinic $BiVO_4$, Chem. Mater. 27 (2015) 3593–3600.
[9] H.S. Park, K.E. Kweon, H. Ye, E. Paek, G.S. Hwang, A.J. Bard, Factors in the metal doping of $BiVO_4$ for improved photoelectrocatalytic activity as studied by scanning electrochemical microscopy and first-principles density-functional calculation, J. Phys. Chem. C 115 (2011) 17870–17879.
[10] M. Long, W. Cai, H. Kisch, Visible light induced photoelectrochemical properties of *n*-BiVO4 and *n*-$BiVO_4$/*p*-Co_3O_4, J. Phys. Chem. C 112 (2008) 548–554.
[11] S.K. Cho, H.S. Park, H.C. Lee, K.M. Nam, A.J. Bard, Metal doping of $BiVO_4$ by composite electrodeposition with improved photoelectrochemical water oxidation, J. Phys. Chem. C 117 (2013) 23048–23056.
[12] S.K. Pilli, T.E. Furtak, L.D. Brown, T.G. Deutsch, J.A. Turner, A.M. Herring, Cobalt-phosphate (Co-Pi) catalyst modified Mo-doped $BiVO_4$ photoelectrodes for solar water oxidation, Energy Environ. Sci. 4 (2011) 5028–5034.
[13] X. Zhang, Y. Zhang, X. Quan, S. Chen, Preparation of Ag doped $BiVO_4$ film and its

enhanced photoelectrocatalytic (PEC) ability of phenol degradation under visible light, J. Hazard. Mater. 167 (2009) 911–914.
[14] C. Yin, S. Zhu, Z. Chen, W. Zhang, J. Gu, D. Zhang, One step fabrication of C-doped $BiVO_4$ with hierarchical structures for a high-performance photocatalyst under visible light irradiation, J. Mater. Chem. A 1 (2013) 8367–8378.
[15] S. Obregón, G. Colón, Heterostructured Er^{3+} doped $BiVO_4$ with exceptional photocatalytic performance by cooperative electronic and luminescence sensitization mechanism, Appl. Catal. B 158 (2014) 242–249.
[16] M. Wang, Q. Liu, Y. Che, L. Zhang, D. Zhang, Characterization and photocatalytic properties of N-doped $BiVO^4$ synthesized via a sol–gel method, J. Alloys Compd. 548 (2013) 70–76.
[17] G. Tan, L. Zhang, H. Ren, J. Huang, W. Yang, A. Xia, Microwave hydrothermal synthesis of N-doped $BiVO_4$ nanoplates with exposed (040) facets and enhanced visible-light photocatalytic properties, Ceram. Int. 40 (2014) 9541–9547.
[18] W.J. Jo, J.W. Jang, K. j. Kong, H.J. Kang, J.Y. Kim, H. Jun, K. Parmar, J.S. Lee, Phosphate doping into monoclinic $BiVO_4$ for enhanced photoelectrochemical water oxidation activity, Angew. Chem. Int. Ed. 51 (2012) 3147–3151.
[19] W. Luo, J. Wang, X. Zhao, Z. Zhao, Z. Li, Z. Zou, Formation energy and photoelectrochemical properties of $BiVO_4$ after doping at Bi^{3+} or V^{5+} sites with higher valence metal ions, Phys. Chem. Chem. Phys. 15 (2013) 1006–1013.
[20] Z. Jiang, Y. Liu, T. Jing, B. Huang, X. Zhang, X. Qin, Y. Dai, M.-H. Whangbo, Enhancing the photocatalytic activity of $BiVO_4$ for oxygen evolution by ce doping: Ce^{3+} ions as hole traps, J. Phys. Chem. C 120 (2016) 2058–2063.
[21] P. Giannozzi, S. Baroni, N. Bonini, M. Calandra, R. Car, C. Cavazzoni, D. Ceresoli, G.L. Chiarotti, M. Cococcioni, I. Dabo, QUANTUM ESPRESSO: a modular and open-source software project for quantum simulations of materials, J. Phys. Condens. Matter 21 (2009) 395502.
[22] Atomistix ToolKitversion. 0, QuantumWise A/S. 2017. (https://quantumwise.com).
[23] K. Momma and F. Izumi, An integrated three-dimensional visualization system VESTA using wxWidgets Commision Crystallogr. Comput., IUCr Newslett, 2006. 106–119.
[24] Virtual NanoLabversion.0, QuantumWise A/S, 2017 (https://quantumwise.com).
[25] A. Sleight, H.-Y. Chen, A. Ferretti, D. Cox, Crystal growth and structure of $BiVO_4$, Mater. Res. Bull. 14 (1979) 1571–1581.
[26] A.H. Larsen, M. Vanin, J.J. Mortensen, K.S. Thygesen, K.W. Jacobsen, Localized atomic basis set in the projector augmented wave method, Phys. Rev. B 80 (2009) 195112.
[27] G. Xi, J. Ye, Synthesis of bismuth vanadate nanoplates with exposed {001} facets and enhanced visible-light photocatalytic properties, Chem. Commun. 46 (2010) 1893–1895.
[28] W.H. Press, Numerical recipes, The Art of Scientific Computing, 3rd edition, Cambridge University Press, 2007.
[29] S.N.F.M. Nasir, H. Ullah, M. Ebadi, A.A. Tahir, J.S. Sagu, M.A. Mat Teridi, New insights into Se/$BiVO_4$ heterostructure for photoelectrochemical water splitting: a combined experimental and DFT study, J. Phys. Chem. C 121 (2017) 6218–6228.
[30] F. Tran, P. Blaha, Accurate band gaps of semiconductors and insulators with a semilocal exchange-correlation potential, Phys. Rev. Lett. 102 (2009) 226401.
[31] A.J. Rettie, H.C. Lee, L.G. Marshall, J.-F. Lin, C. Capan, J. Lindemuth, J.S. McCloy, J. Zhou, A.J. Bard, C.B. Mullins, Combined charge carrier transport and photoelectrochemical characterization of $BiVO_4$ single crystals: intrinsic behavior of a complex metal oxide, J. Am. Chem. Soc. 135 (2013) 11389–11396.
[32] Z. He, Y. Shi, C. Gao, L. Wen, J. Chen, S. Song, BiOCl/$BiVO_4$ p–n heterojunction with enhanced photocatalytic activity under visible-light irradiation, J. Phys. Chem. C 118 (2013) 389–398.
[33] D. Wang, R. Li, J. Zhu, J. Shi, J. Han, X. Zong, C. Li, Photocatalytic water oxidation on $BiVO_4$ with the electrocatalyst as an oxidation cocatalyst: essential relations between electrocatalyst and photocatalyst, J. Phys. Chem. C 116 (2012) 5082–5089.
[34] S. Sun, W. Wang, D. Li, L. Zhang, D. Jiang, Solar light driven pure water splitting on quantum sized $BiVO_4$ without any cocatalyst, ACS Catal. 4 (2014) 3498–3503.